IEEE Access
Multidisciplinary | Rapid Review | Open Access Journal

Received May 29, 2019, accepted July 1, 2019, date of publication July 18, 2019, date of current version August 14, 2019.

Digital Object Identifier 10.1109/ACCESS.2019.2929738

A Simplified Form of Beam Spread Function in Underwater Wireless Optical Communication and Its Applications

PRAKRITI SAXENA, (Student Member, IEEE), AND MANAV R. BHATNAGAR, (Senior Member, IEEE)
Department of Electrical Engineering, Indian Institute of Technology Delhi, New Delhi 110016, India

Corresponding author: Prakriti Saxena (prakriti1192@gmail.com)

This work was supported in part by the Media Laboratory Asia (Sir Visvesvaraya Young Faculty Research Fellowship) through the Ministry of Electronics and Information Technology (MeiTY), Government of India, and in part by the Science and Engineering Research Board (SERB), Department of Science and Technology (DST), Government of India, through Extramural Research (EMR) Funding Scheme for "Quantized Feedback Based Collocated and Distributed Wireless Communication Systems: Study and Hardware Implementation" under Project EMR/2016/000592.

ABSTRACT Underwater wireless optical communication (UWOC) refers to the transmission of data in unguided water medium through optical carriers. Beam spread function (BSF) characterizes the amount of light irradiance received at the receiver as a function of receiver's distance from main beam axis for a particular link length. The existing form of BSF includes multiple integrals which are burdensome to use for mathematical analysis. Because of this, it gets very difficult to employ the existing form of BSF to derive non-integral expressions for bit error rate (BER), capacity, and outage probability of UWOC systems. Moreover, it is very difficult to find any insight into the UWOC systems based on this integral form of BSF. In this paper, we derive a simplified power series expression of BSF by solving the existing integral form. Closed-form expressions of BSF with some approximations, which simplify the derived power series expression, are also provided as special cases. Important insights regarding the behavior of BSF are also obtained from the derived simplified forms. Furthermore, closed-form expressions of BER, capacity, and outage probability of the UWOC system, taking the effect of scattering, absorption, and misalignment in consideration, are also derived.

INDEX TERMS Beam spread function, bit error rate, capacity, log-normal distribution, outage probability, scattering phase function, underwater optical communication, volume scattering function.

I. INTRODUCTION

Since earth's surface is mainly water, we need technologies that can help with communications inside water. Underwater wireless communication (UWC) systems are very useful for study of the environment inside the ocean [1]. Further, UWC systems are very helpful in vehicle-to-vehicle communication inside water. Many technologies such as radio frequency (RF) communication [2], [3] and underwater acoustic communication (UWAC) [4], [5] are widely being used for wireless communication inside water. Despite strong attenuation, acoustic waves can travel a distance of about 10-90 km inside water [6], [7]; the attenuation gets stronger with frequency [8]. As shown in [9], the bandwidth of the acoustic signals depends on the transmission distance. As the distance increases, the bandwidth gets severely limited, thus, rendering poor data rate. The underwater RF communication provides relatively smoother air/water transition than other forms of communication; and it is more tolerant towards water turbulence and turbidity. However, the RF communication can be used only for short links, as the sea water containing salt acts as a conductive transmission medium; hence, RF waves can propagate up to a few meters at extra low frequency (30-300 Hz) [10], [11]. Transmission bandwidth of optical signal in underwater optical communication (UWOC) is higher as compared to RF communication and UWAC, thus providing much higher data rate. Since optical signals are high frequency signals, they can employ

The associate editor coordinating the review of this manuscript and approving it for publication was Miaowen Wen.

high bandwidth for UWOC [11]. To the best of author's knowledge, currently a data rate of 4.8 Gbits/s over a 5.5 m watertank transmission link can be achieved [11]. A study of spatial and temporal dispersion effects of UWOC links under various modulation techniques, coding schemes, and water conditions is done in [12]. In UWOC the received optical signal experiences a minuscule delay, which further makes it possible to implement real-time applications such as transmission of video signals inside water. Further, UWOC also provides better security than UWAC and RF communication. Since UWOC utilizes line-of-sight (LOS) to establish communication between transmitter and receiver, eavesdropping of the transmitted signals is difficult. Moreover, RF and UWAC schemes require bulky and costly transceivers, whereas UWOC needs photodiodes and laser diodes as transceivers which are relatively smaller and cheaper. This may further lead to a large scale commercialization of UWOC [11]. Although UWOC has many advantages over UWAC and RF communications, it certainly has few limitations, e.g. light signal inside water suffers from severe scattering and absorption [13], [14]. In order to overcome this problem, the wavelength of the transmitted signal is selected in the blue-green spectrum (which offers the least attenuation in visible range) [15], [16]. However, due to the continuous interaction of photons and water molecules, scattering and absorption can badly attenuate the signal even in blue-green spectrum [15], [16]. Since wireless optical communication needs LOS, even a small misalignment can influence the performance of the system greatly [17]. For deep sea applications where solar energy is negligible (for a depth $>$600 m) [18], we need strong battery backup inside water to keep the instruments working.

A. MOTIVATION

Scattering is a process in which photon particles deviate from their original path interacting with the suspended particles in water. Whereas, absorption is a process in which photon particles lose their energy after colliding with the suspended particles in water. Both phenomena lead to a reduced optical power, thereby diminishing the signal-to-noise ratio (SNR) at a particular link length. It is important to consider the effect of scattering, because for a well-collimated beam the nonscattered light is only captured when the transceivers are perfectly aligned. With the increasing link length, more number of photons interact with the suspended particles present in water; resulting in a severe scattering. When the link length becomes extremely large, the receiver receives only the scattered component [19]. Misalignment loss in UWOC occurs due to movements caused by underwater vehicles, ocean currents, and other turbulent sources. A constant tracking between the transmitter and receiver is required to maintain LOS. Misalignment loss further degrades the SNR of the system. In order to get an uninterrupted communication in UWOC, a communication engineer needs to study the process that governs both scattered and nonscattered light to determine other parameters such as range, pointing, acquisition, and tracking. For free space optical (FSO) communication, the exponential pointing error model is widely employed in the literature [20], [21]. However, the same model cannot be used for UWOC.

Beam spread function (BSF) indicates the total scattered profile of transmitted optical beam. It shows the amount of light irradiance received as a function of distance of the receiver from the main beam axis at a particular link length. Thus, it gives a combined effect of two independent phenomena in a single equation. It has also been mentioned in literature that the link misalignment in UWOC is modeled through BSF [22]–[25]. In [22], the performance of link misalignment in UWOC is studied and a relation of transmit power, link range, and receiver offset is derived. However, no non-integral form of the expression is given there. Link misalignment caused by light source properties such as divergence angle and elevation angle, and its effect on the spatial and temporal spreading of light is discussed in [21]. The results are derived using simulation methods and no non-integral form is provided. The effect of random sea slope with link misalignment on a downlink UWOC system is delineated in [25]. The spatial effect of scattering on the optical signal and its impact on the received irradiance is determined by the BSF, and its ramification on pointing, tracking, and link misalignment is studied in [23]. However, the current expression of BSF available in literature [24, Eq. (14)] is in integral form; and it is very tedious to deal with the current form for further mathematical explorations. It would be cumbersome to derive physical insights into the UWOC system by using the integral form of BSF for study of the effect of scattering, misalignment loss, and oceanic turbulence in terms of performance metrics such as bit error rate (BER), capacity, and outage probability. Therefore, there is a need for a simplified form of BSF which can be used to predict the system performance more conveniently.

In this paper, we simplify the existing BSF and provide a power series based simplified solution for the misalignment loss in UWOC. The nature of BSF for different parameters is studied using this simplified form. By using the derived form of BSF, we are able to explore some special cases for obtaining closed-form expressions of BSF for few practically useful conditions; that greatly helps in obtaining useful insights into the UWOC system and further adding to the intuitive understanding of such systems. Moreover, we derive an expression of instantaneous SNR and using this, the probability density function (pdf) of the received SNR is also obtained. Furthermore, closed-form expressions of BER, average channel capacity, and outage probability for a UWOC system with Log-Normal oceanic turbulence and misalignment loss are derived, which are not available in literature to the best of authors' knowledge.

The rest of the paper is organized as follows. The basics of BSF are given in Section II. The derivation of the simplified closed-form expression for BSF is provided in Section III. In Section IV, we calculate the BER and the average channel capacity of UWOC with fading and pointing error. We further

TABLE 1. List of mathematical notation.

φ	Angle between scattered and nonscattered part of light	λ	Wavelength
P_{ab}	Absorbed power	P_{sc}	Scattered power
P_{tr}	Power of optical beam which is neither scattered nor absorbed	P_{in}	Transmitted power of optical beam from source
P_{RX}	Total power received	$A(\lambda)$	Absorptance
$B(\lambda)$	Scatterance	$T(\lambda)$	Transmittance
$a(\lambda)$	Absorption coefficient	$b(\lambda)$	Scattering coefficient
$\mathscr{P}(\varphi)$	Scattering phase function (SPF)	g	Asymmetry parameter
$\mathscr{V}(\varphi)$	Volume scattering function (VSF)	ζ_{rec}	Link length
δ	Distance of receiver from origin	Δ	Diameter of receiver aperture
$V_0(\zeta_{rec})$	Variance of Gaussian source in free space	$J_\upsilon(\cdot)$	Bessel function of the first kind with υ_{th} order
${}_1F_2(\cdot;\cdot,\cdot;\cdot)$	Hypergeometric function	$(\mathscr{V})_n$	Pochhamer Symbol
$\mathscr{R}$	Responsivity	$Pr(\cdot)$	Probability

derive the pdf of SNR using the simplified form of BSF and find the outage probability of the considered system. The numerical results are discussed in Section V and some conclusions are drawn in Section VI. The paper also contains three appendices.

A comprehensive list of all the mathematical notations used in this paper is given in Table 1.

II. BSF PRELIMNARIES

The optical properties of water are broadly classified into two categories: Inherent Optical Properties (IOP) and Apparent Optical Properties (AOP) [26]–[28]. IOPs depend only on medium and are independent of the geometry of ambient light in the medium. The two significant IOPs are $a(\lambda)$ and volume scattering function (VSF) [19], [29]. On the other hand, AOPs [26] depend upon both the medium and the direction of the ambient light field. Quite frequently used AOPs are the various reflectances, average cosines, and diffuse attenuation coefficients. Radiative transfer theory provides a connection between the IOPs and the AOPs.

Figure 1 shows a small volume ΔV of water with thickness Δr [30]. A monochromatic beam of light with power $P_{in}(\lambda)$ W-nm^{-1} is incident from one side of the column; $P_{ab}(\lambda)$ is absorbed by the water column while $P_{sc}(\lambda)$ gets scattered and $P_{tr}(\lambda)$ remains unaffected. It can be seen from the figure that, $P_{in}(\lambda) = P_{ab}(\lambda) + P_{sc}(\lambda) + P_{tr}(\lambda)$. Let $A(\lambda) = P_{ab}(\lambda)/P_{in}(\lambda)$ be the fraction of incident power absorbed in the given volume. Similarly, $B(\lambda) = P_{sc}(\lambda)/P_{in}(\lambda)$ is the fraction of incident light power scattered in the given volume and $T(\lambda) = P_{tr}(\lambda)/P_{in}(\lambda)$ is defined as the fraction of light power which is unscattered and unabsorbed by the medium. The IOPs commonly used in UWOC are $a(\lambda)$ and $b(\lambda)$ which are equal to $A(\lambda)$ and $B(\lambda)$, respectively, per unit distance in the water column.

It is common to use beam attenuation coefficient to measure the optical loss in turbid water; this is defined for

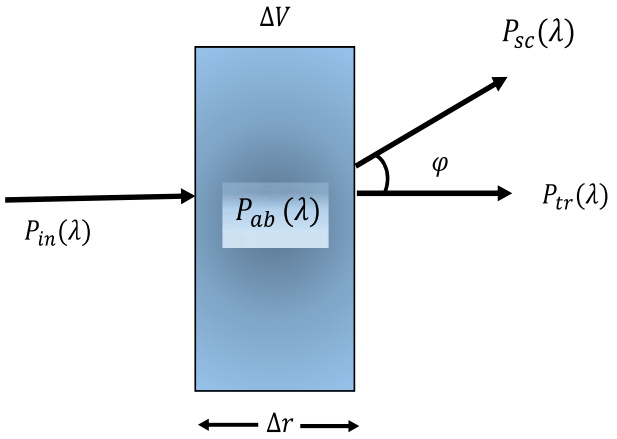

FIGURE 1. Geometry to define inherent optical properties.

non-scattered light. Another parameter that indicates the turbidity of water is diffused attenuation constant [26], [27]. It shows how visible light penetrates the water column in blue and green spectrum. It is directly dependent upon the presence of scattering particles in water column. At a longer link length, the receiver may just be receiving only the scattered part of light beam. VSF, i.e., $\mathcal{V}(\varphi)$ tells how the medium scatters light, it is defined as the scattered intensity per unit incident irradiance per unit volume of water at a particular angle ϕ [30], [31]; integrating $\mathcal{V}(\varphi)$ over all directions yields $b(\lambda)$. The integration is often divided into forward scattering and backward scattering. Normalizing $\mathcal{V}(\varphi)$ by $b(\lambda)$ gives the scattering phase function (SPF), i.e., $\mathcal{P}(\varphi)$ [32]–[34]. The Henyey Greenstein parameter which is represented by g is the average cosine of the scattering angle over all directions. The asymmetry parameter provides an easy way to measure the shape of the phase function.

The total scattering profile of a collimated beam can be described by the BSF. The geometry of the

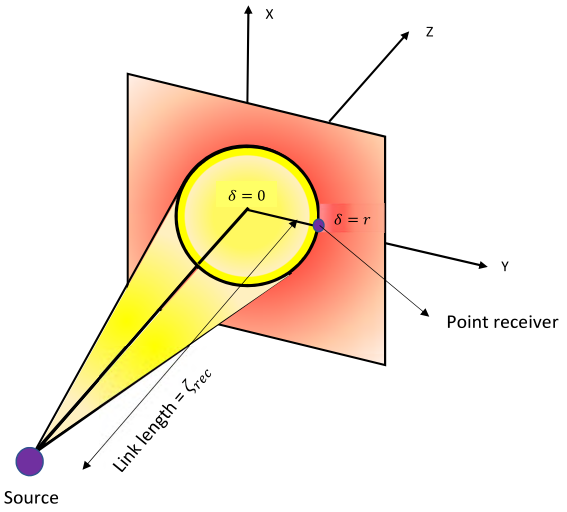

FIGURE 2. Geometry to compute BSF function.

transmitter (source) and a point receiver inside water for calculation of the BSF [35], is shown in Fig. 2. It can be seen from the figure that the source and the point receiver are ζ_{rec} m away from each other. If the receiver is at origin, i.e., $\delta = 0$, then the source and receiver are perfectly aligned. If the receiver is at some distance δ from the origin, then a misalignment between the source and the receiver occurs. So the light intensity, received as a function of δ on a plane which is ζ_{rec} m away from the source, is given by the BSF [36], [37]. As the beam passes through water, the transmitted optical beam will spread due to scattering and its power will reduce due to absorption. Therefore, the analytical formulation of the BSF requires the solution of a complex radiative transfer equation [38], [39]. However, by considering small angle approximation (SAA), [40], [41], researchers have come up with an integral form of BSF [22]–[24], [42], given by:

$$\begin{aligned}&\mathrm{BSF}(\delta, \zeta_{rec})\\ &= E_0(\delta, \zeta_{rec})e^{-c\zeta_{rec}} + \frac{1}{2\pi}\int_0^{\infty} E_0(\nu, \zeta_{rec}) \times\ e^{-c\zeta_{rec}}\\ &\quad\times \left\{\exp\left[\int_0^{\zeta_{rec}} b\mathcal{P}\big(\nu(\zeta_{rec}-\zeta)\big)d\zeta\right]-1\right\} J_0(\nu\delta)\nu d\nu, \quad (1)\end{aligned}$$

where c is the attenuation coefficient, b is the scattering coefficient, (ν, ζ_{rec}) representing the spatial frequency domain, and (δ, ζ_{rec}) representing the spatial coordinate system; $\mathcal{P}\big(\nu(\zeta_{rec}-\zeta)\big)$ is the Hankel Transform of the SPF; $E_0(\nu, \delta)$ is the laser source Gaussian irradiance distribution in free space in frequency domain at ζ_{rec} is defined as:

$$E_0(\nu, \zeta_{rec}) \triangleq P_{in}(\lambda)\exp\left[-\frac{V_0(\zeta_{rec})\nu^2}{2}\right]. \quad (2)$$

Equation (2) is given in spatial frequency domain, and therefore, the 2-D Fourier transform is required to convert it to the spatial coordinate system. However, the Hankel transform is generally used in place of 2-D Fourier transform in order to simplify the calculations [43]. The Hankel Transform of (2) is given by:

$$E_0(\delta, \zeta_{rec}) = \frac{P_{in}(\lambda)}{2\pi V_0(\zeta_{rec})}\exp\left(\frac{-\delta^2}{2V_0(\zeta_{rec})}\right). \quad (3)$$

A. MOTIVATION FOR A SIMPLIFIED FORM OF BSF

The aforementioned equation of BSF given by (1) is in integral form which includes an infinite integral, a finite integral, and Hankel transform of scattering phase function which involves another infinite integral. The BSF is useful for studying the effect of scattering and misalignment loss in UWOC system. Note that BSF depends only upon the IOPs and not on misalignment loss; however, two can be convolved in one equation that provides a single attenuation term at the receiver. Thus, a simpler form is necessary in order to understand the effect of scattering and misalignment loss through BSF function over the performance of UWOC systems.

Due to the existing integral form of BSF as shown in (1), it becomes nearly impossible to consider its effect in the performance analysis of the system. Because of this, BER, capacity, and outage probability analysis of UWOC under the influence of scattering and misalignment errors have not been thoroughly performed, to the best of our knowledge. It is necessary to obtain the pdf of oceanic turbulence under the combined effect of misalignment loss and oceanic turbulence to study the effect of scattering in UWOC. Due to the existing complicated integral form of the BSF, it is difficult to get a simple form of the combined pdf of oceanic turbulence and BSF without any integrals. In [23], the BER performance under the combined influence of surface sea slope and misalignment loss is shown; however, the BER expression contains multiple infinite integrals due to the complex integral form of BSF. Therefore, it is difficult to compute analytical BER of the system. Further, deriving useful insights of the system is not so straight forward using the integral expression of BSF.

This has motivated us to obtain a simplified solution of the BSF. Using this derived expression, some special cases help us to strengthen the intuitive understanding of UWOC systems which cannot be easily obtained using the integral form of BSF. Moreover, it will be shown in (35) that the instantaneous SNR (which takes misalignment loss into account) is a function of BSF. Hence, with the existing integral form of BSF, it gets really difficult to compute the pdf of SNR. Hence, the outage probability calculation also gets involved. Further, having a simplified form of BSF helps in getting a simpler form of BER and capacity, which can be further used to predict the system performance such as SNR loss and link design.

III. COMPUTATION OF BSF

In this section we will compute a simplified form of existing BSF equation given in (1).

In order to study the effect of scattering, the Henyey-Greenstein (HG) function is used which varies from back

scattering to forward scattering by the variation of g, whose value varies as $-1 < g < 1$. When $g < 0$, back scattering dominates; whereas, for $g > 0$, forward scattering dominates. In this work, we use $g = 0.924$ [32], [44], which is applicable for all the water types. SPF is modeled by HG function [11] in UWOC for a given wavelength and represented as:

$$\mathcal{P}(\varphi) = \frac{1-g^2}{4\pi(1+g^2-2g\cos\varphi)^{3/2}}. \tag{4}$$

First, we need to find the Hankel transform of SPF at a given wavelength λ:

$$\mathcal{P}(\nu) = \frac{1}{2}\int_0^{\pi} \frac{(1-g^2)J_0(\nu\varphi)\varphi}{4\pi(1+g^2-2g\cos\varphi)^{3/2}}d\varphi. \tag{5}$$

It should be noted that the integration in (5) has a complex form. In order to get a closed-form, we need to use binomial approximation [45]; after some algebra, (5) can be written as:

$$\mathcal{P}(\nu) = \mathcal{K}\int_0^{\pi} J_0(\nu\varphi)\varphi\Big(1+\frac{3g}{1+g^2}\cos\varphi d\varphi\Big), \tag{6}$$

where $\mathcal{K} = (1-g^2)/(8\pi(1+g^2)^{3/2})$. Let us rewrite (6) as:

$$\mathcal{P}(\nu) = I_1 + I_2, \tag{7}$$

where

$$I_1 = \mathcal{K}\int_0^{\pi} J_0(\nu\varphi)\varphi d\varphi, \tag{8a}$$

$$I_2 = \frac{3g\mathcal{K}}{1+g^2}\int_0^{\pi} \varphi\cos\varphi J_0(\nu\varphi)d\varphi. \tag{8b}$$

In order to solve the two integrations in (8), the series form of $J_0(\cdot)$ [46] is used; it will be shown in Section V that the infinite series converges easily for a small number of summation terms. Though the series form of $J_0(\cdot)$ renders the analytical performance result in the power series; however, its fast convergence simplifies the integral to a large extent. By using the series form of $J_0(\nu)$, we can rewrite (8a) as follows:

$$I_1 = \mathcal{K}\int_0^{\pi}\sum_{m=0}^{\infty}\frac{(-1)^m}{m!\Gamma(m+1)}\Big(\frac{\nu\varphi}{2}\Big)^{2m}\varphi d\varphi. \tag{9}$$

Solving and simplifying (9), we get:

$$I_1 = \frac{\mathcal{K}\pi}{\nu}\sum_{m=0}^{\infty}\frac{(-1)^m}{m!(m+1)\Gamma(m+1)}\Big(\frac{\pi\nu}{2}\Big)^{2m+1}. \tag{10}$$

Again using [46, Eq. (42)], (10) can be written as follows:

$$I_1 = \frac{\mathcal{K}\pi}{\nu}J_1(\pi\nu). \tag{11}$$

To solve I_2, we utilize the series expression for the Bessel function [46] which yields:

$$I_2 = \frac{3\mathcal{K}g}{1+g^2}\sum_{m=0}^{\infty}\frac{(-1)^m}{m!\Gamma(m+1)}\Big(\frac{\nu}{2}\Big)^{2m}\int_0^{\pi}\varphi^{2m+1}\cos\varphi d\varphi. \tag{12}$$

It is shown in Appendix A that the integral term in (12) gets simplified as:

$$\int_0^{\pi}\varphi^{2m+1}\cos(\varphi)d\varphi = \frac{\pi^{2m+2}}{(2m+2)}{}_1F_2\Big(1+m;\frac{1}{2},2+m;\frac{-\pi^2}{4}\Big). \tag{13}$$

From (12) and (13), we get:

$$I_2 = \frac{3\mathcal{K}g}{1+g^2}\sum_{m=0}^{\infty}\frac{(-1)^m}{m!\Gamma(m+1)}\Big(\frac{\nu}{2}\Big)^{2m}\frac{\pi^{2m+2}}{(2m+2)} \times{}_1F_2\Big(1+m;\frac{1}{2},2+m;\frac{-\pi^2}{4}\Big). \tag{14}$$

Substituting (11) and (14) in (7), we have:

$$\mathcal{P}(\nu) = \frac{(1-g^2)}{8(1+g^2)^{3/2}\nu}J_1(\pi\nu) + \frac{3g(1-g^2)}{8\pi(1+g^2)^{5/2}} \times\sum_{m=0}^{\infty}\frac{(-1)^m}{m!\Gamma(m+1)}\Big(\frac{\nu}{2}\Big)^{2m}\frac{\pi^{2m+2}}{2m+2} \times{}_1F_2\Big(1+m;0.5,2+m;\frac{-\pi^2}{4}\Big). \tag{15}$$

Remark 1: Equation (15) provides a very accurate and simplified form for the Hankel Transform of SPF. Although (15) is in the form of infinite series but it converges quickly for finitely small values of m which will be evident from Table 3. We have shown in Appendix B.

Now, $\mathcal{P}(\nu(\zeta_{rec}-\zeta))$ can be obtained by substituting $\nu(\zeta_{rec}-\zeta)$ in place of ν in (15). Further, to get a simplified form of BSF given by (1), we need to solve the following integration:

$$I' = \int_0^{\zeta_{rec}} b\mathcal{P}(\nu(\zeta_{rec}-\zeta))d\zeta = I_3 + I_4, \tag{16}$$

where

$$I_3 = \mathcal{K}b\pi\int_0^{\zeta_{rec}}\frac{J_1(\pi\nu(\zeta_{rec}-\zeta))}{\nu(\zeta_{rec}-\zeta)}d\zeta, \tag{17a}$$

$$I_4 = \sum_{m=0}^{\infty}\frac{3b\mathcal{K}g(-1)^m\pi^{2m+2}}{(1+g^2)m!\Gamma(m+1)(2m+2)} \times{}_1F_2\Big(1+m;0.5,2+m;\frac{-\pi^2}{4}\Big) \times\int_0^{\zeta_{rec}}\Big(\frac{\nu(\zeta_{rec}-\zeta)}{2}\Big)^{2m}d\zeta. \tag{17b}$$

The integration in (17a) can be evaluated as shown in Appendix C:

$$\int_0^{\zeta_{rec}}\frac{J_1(\pi\nu(\zeta_{rec}-\zeta))}{\nu(\zeta_{rec}-\zeta)}d\zeta = \frac{\pi\zeta_{rec}}{2}{}_1F_2\Big(\frac{1}{2};\frac{3}{2},2;\frac{-\nu\zeta_{rec}^2\pi^2}{4}\Big). \tag{18}$$

Using (18), I_3 is simplified as:

$$I_3 = \frac{\mathcal{K}b\pi^2\zeta_{rec}}{2}{}_1F_2\Big(\frac{1}{2};\frac{3}{2},2;\frac{-\nu^2\zeta^2\pi^2}{4}\Big). \tag{19}$$

$$\mathrm{BSF}(\delta,\zeta_{rec}) = \frac{P_{in}(\lambda)}{2\pi V_0(\zeta_{rec})}\exp\Big(\frac{-\delta^2}{2\,V_0(\zeta_{rec})}\Big)\exp(-c\zeta_{rec}) + \frac{1}{2\pi}\sum_{i=1}^{n} w_i e^{x_i} P_{in}(\lambda)\exp\Big[-\frac{V_0(\zeta_{rec})x_i^2}{2}\Big]\exp(-c\zeta_{rec})$$
$$\Big\{\exp\Big[\frac{\mathcal{K}b\pi^2\zeta_{rec}}{2}\times {}_1F_2\Big(\frac{1}{2};\frac{3}{2},2;\frac{-x_i\zeta_{rec}^2\pi^2}{4}\Big) + \sum_{m=0}^{\infty}\frac{3b\mathcal{K}g(-1)^m\pi^{2m+2}}{(1+g^2)m!\Gamma(m+1)(2m+2)}\Big(\frac{x_i}{2}\Big)^{2m}\Big(\frac{\zeta_{rec}^{2m+1}}{2m+1}\Big)$$
$$\times {}_1F_2\Big(1+m;\frac{1}{2},2+m;\frac{-\pi^2}{4}\Big)\Big] - 1\Big\}J_0(x_i\delta) \tag{25}$$

$$\mathrm{BSF}(\delta,\zeta_{rec}) = P_{ns} + \frac{1}{2\pi}\sum_{i=1}^{n} w_i e^{x_i} P_{in}(\lambda)\exp\Big(\frac{-V_0(\zeta_{rec})x_i^2}{2}\Big)\exp(-c\zeta_{rec})\Big\{\exp\Big[\frac{\mathcal{K}b\pi^2\zeta_{rec}}{2}{}_1F_2\Big(\frac{1}{2};\frac{3}{2},2;\frac{-x_i\zeta_{rec}^2\pi^2}{4}\Big)$$
$$-\frac{0.6079b\mathcal{K}g\zeta_{rec}}{(1+g^2)}\Big] - 1\Big\}J_0(x_i\delta) \tag{26}$$

$$\mathrm{BSF}(\delta,\zeta_{rec}) = \frac{1}{2\pi}\sum_{i=1}^{n} w_i e^{x_i} P_{in}(\lambda)\exp\Big[-\frac{V_0(\zeta_{rec})x_i^2}{2}\Big]\exp(-c\zeta_{rec})\Big\{\exp\Big[\frac{\mathcal{K}b\pi^2\zeta_{rec}}{2}{}_1F_2\Big(\frac{1}{2};\frac{3}{2},2;\frac{-x_i\zeta_{rec}^2\pi^2}{4}\Big)$$
$$+\sum_{m=0}^{\infty}\frac{3b\mathcal{K}g(-1)^m\pi^{2m+2}}{(1+g^2)m!\Gamma(m+1)(2m+2)}\times\Big(\frac{x_i}{2}\Big)^{2m}\frac{\zeta_{rec}^{2m+1}}{2m+1}{}_1F_2\Big(1+m;\frac{1}{2},2+m;-\frac{\pi^2}{4}\Big)\Big] - 1\Big\}J_0(x_i\delta). \tag{27}$$

$$\mathrm{BSF}(\delta,\zeta_{rec}) = P_{ns} + \frac{1}{2\pi}\sum_{i=1}^{n} w_i e^{x_i} P_{in}(\lambda)\exp\Big(\frac{-V_0(\zeta_{rec})x_i^2}{2}\Big)\exp(-c\zeta_{rec})\Big\{\exp\Big[\frac{\mathcal{K}b\pi^2\zeta_{rec}}{2}{}_1F_2\Big(\frac{1}{2};\frac{3}{2},2;\frac{-x_i\zeta_{rec}^2\pi^2}{4}\Big)$$
$$-\frac{0.6079b\mathcal{K}g\zeta_{rec}}{(1+g^2)}\Big] - 1\Big\} \tag{28}$$

$$\mathrm{BSF}(\delta,\zeta_{rec}) = \frac{1}{2\pi}\sum_{i=1}^{n} w_i e^{x_i} P_{in}(\lambda)\exp\Big(\frac{-V_0(\zeta_{rec})x_i^2}{2}\Big)\exp(-c\zeta_{rec})\Big\{\exp\Big[\frac{\mathcal{K}b\pi^2\zeta_{rec}}{2}{}_1F_2\Big(\frac{1}{2};\frac{3}{2},2;\frac{-x_i\zeta_{rec}^2\pi^2}{4}\Big)$$
$$-\frac{0.6079b\mathcal{K}g\zeta_{rec}}{(1+g^2)}\Big] - 1\Big\}\times\sqrt{\frac{2}{\pi(x_i\delta)}}\Big(\cos\big(x_i\delta-\frac{\pi}{4}\big)\Big). \tag{29}$$

Further, I_4 can be computed easily:

$$I_4 = \sum_{m=0}^{\infty}\frac{3b\mathcal{K}g(-1)^m\pi^{2m+2}}{(1+g^2)m!\Gamma(m+1)(2m+2)}\Big(\frac{\nu}{2}\Big)^{2m}\frac{\zeta_{rec}^{2m+1}}{2m+1}$$
$$\times {}_1F_2\Big(1+m;\frac{1}{2},2+m;-\frac{\pi^2}{4}\Big). \tag{20}$$

Thus, I' is given by substituting (19), and (20) in (16):

$$I' = \frac{\mathcal{K}b\pi^2\zeta_{rec}}{2}{}_1F_2\Big(\frac{1}{2};\frac{3}{2},2;\frac{-\nu^2\zeta^2\pi^2}{4}\Big) + \sum_{m=0}^{\infty}\frac{3b\mathcal{K}g(-1)^m}{(1+g^2)m!}$$
$$\times\Big(\frac{\nu}{2}\Big)^{2m}\frac{\zeta_{rec}^{2m+1}\pi^{2m+2}}{\Gamma(m+1)(2m+1)(2m+2)}{}^1$$
$$F_2\Big(1+m;\frac{1}{2},2+m;-\frac{\pi^2}{4}\Big). \tag{21}$$

By using (15), and (21), (1) is expressed as:

$$\mathrm{BSF}(\delta,\zeta_{rec}) = E_0(\delta,\zeta_{rec})\exp(-c\zeta_{rec}) + \frac{1}{2\pi}\int_0^{\infty}E_0(\nu,\zeta_{rec})$$
$$\times\exp(-c\zeta_{rec})\{\exp(I')-1\}J_0(\nu\delta)\nu d\nu. \tag{22}$$

Remark 2: The integration in (22) can be approximated using Gauss-Laguerre Quadrature [47], [48] as:

$$\int_0^{\infty}\exp(-x)f(x)dx \cong \sum_{i=1}^{n} w_i f(x_i), \tag{23}$$

where x_i is the i_{th} root of Laguerre polynomial $L_n(x)$ [48] of order n and the weight w_i is given by:

$$w_i = \frac{x_i}{(n+1)^2[L_{n+1}(x_i)]^2}$$

The value of x_i and weights w_i is given in [47].

The integral in (22) be represented in a form similar to the left hand side of (23):

$$J = \int_0^{\infty}E_0(\nu,\zeta_{rec})\exp(-c\zeta_{rec})\{\exp(I')-1\}J_0(\nu\delta)\nu d\nu.$$
$$= \int_0^{\infty}g(\nu)\exp(\nu)\exp(-\nu)d\nu$$
$$= \int_0^{\infty}f(\nu)\exp(-\nu)d\nu, \tag{24}$$

where

$$g(\nu) = E_0(\nu,\zeta_{rec})\exp(-c\zeta_{rec})\{\exp(I')-1\}J_0(\nu\delta)\nu\exp(\nu)$$

and $f(\nu) = g(\nu)\exp(\nu)$.

Thus, by using (22) and (24), a simplified form in terms of power series of BSF is given by (25) given at the top of previous page.

We will now discuss some special cases which simplify the derived expression of BSF given by (25) upto a great extent. We also provide accurate closed-form expressions of BSF for different conditions on ζ_{rec} and δ.

1) SMALL ζ_{REC} (e.g. $\zeta_{rec} \leq 2$ m)

When ζ_{rec} is small,[1] e.g.. $\zeta_{rec} \leq 2$ m, we can approximate the infinite series in (25) by substituting $m = 0$. This is because for small ζ_{rec}, the terms of the infinite series in (25) for $m > 0$ become infinitesimally small and can be neglected; hence, we can have an approximate closed-form expression of BSF is given in (26) at the top of previous page, where $P_{ns} = \frac{P_{in}(\lambda)}{2\pi V_0(\zeta_{rec})} \exp\left(\frac{-\delta^2}{2\,V_0(\zeta_{rec})}\right) \exp(-c\zeta_{rec})$.

2) LARGE ζ_{REC} (e.g. $\zeta_{rec} >> 2$ m)

As the value of ζ_{rec} becomes high, the term $\exp(-c\zeta_{rec})$ becomes very small in (25); consequently, the value of P_{ns} is almost negligible and can be ignored. Thus, for high ζ_{rec}, the equation of BSF is given in (27) at the top of previous page.

Remark 3: It can be seen from (27), that for high ζ_{rec}, BSF$(\delta, \zeta_{rec}) \propto J_0(x_i\delta)$. Thus, after a specific value of δ say δ_s, BSF function will start fluctuating. Here δ_s is the value of δ after which the BSF function starts fluctuating. The value of δ_s will be different for different water types and link lengths. Thus, for a given water type, link length, and transmitted power, the UWOC system can tolerate a misalignment only upto δ_s. This conclusion is clearly visible from (27), which is not evident from the already existing BSF expression as given in (1).

3) SMALL δ (e.g. $\delta \leq 2$ M)

For small values of δ, the argument inside Bessel function gets smaller. For small arguments of J_0, i.e., $0 < x_i\delta < 1$, $J_0(x_i\delta) \rightarrow 1$ [50]. Thus, for small values of δ, we can completely ignore the Bessel function.

4) LARGE δ (e.g. $\delta >> 2$ M)

For large values of δ, $\exp\left(\frac{-\delta^2}{2\,V_0(\zeta_{rec})}\right) \rightarrow 0$ and thus, $P_{ns} \rightarrow 0$ which makes BSF$(\delta, \zeta_{rec}) \propto J_0(x_i\delta)$. Also for high δ, the argument of $J_0(x_i\delta)$ gets large enough to approximate $J_0(x_i\delta) \sim \sqrt{2/(\pi x_i\delta)}(\cos(x_i\delta - \pi/4))$. This approximation works well for all values of ζ_{rec} and $\delta > 2$m.

5) SMALL ζ_{REC} AND SMALL δ (e.g. $\zeta_{rec} \leq 2$ m AND $\delta \leq 2$ m)

When both ζ_{rec} and δ are small, we can substitute $m = 0$ in the infinite series and $J_0 \rightarrow 1$ in (25). Thus, we can further simplify the BSF and get a closed-form expression given in (28) at the top of previous page.

6) SMALL ζ_{REC} AND LARGE δ (e.g. $\zeta_{rec} \leq 2$ m AND $\delta >> 2$ m)

For this case, as mentioned for the aforementioned cases, when δ is large and ζ_{rec} is small, $P_{ns} \rightarrow 0$ and thus P_{ns} can be neglected. Further as δ is large, as mentioned in case 3, $J_0(x_i\delta) \rightarrow 1$. Also since, ζ_{rec} is small, $m = 0$ in the infinite series of (25). Therefore, the BSF expression in (25) is further simplified and given in (29) at the top of previous page.

7) LARGE ζ_{REC} AND SMALL δ (e.g. $\zeta_{rec} >> 2$ m AND $\delta \leq 2$ m)

For large ζ_{rec}, $P_{ns} \rightarrow 0$, and for small δ, $J_0(x_i\delta) \rightarrow 1$. Thus, for this case BSF expression in (25) reduces to the expression given in (30) at the top of the next page.

8) LARGE ζ_{REC} AND LARGE δ (e.g. $\zeta_{rec} >> 2$ m AND $\delta >> 2$ m)

For this case also $P_{ns} \rightarrow 0$ and $J_0 x_i\delta \sim \sqrt{2/\pi(x_i\delta)}(\cos(x_i\delta - \pi/4))$. Therefore, BSF can be simplified as (31) which is given at the top of the next page.

The above derived approximations results in a very accurate and simple forms of BSF for various conditions on ζ_{rec} and δ. We have given the approximations for $\zeta_{rec} \leq 2$ m, $\zeta_{rec} >> 2$ m, $\delta \leq 2$ m, and $\delta >> 2$ m. The expressions of BSF received after using the approximations are thoroughly verified by simulations in Section V. The closed-form expressions are very simple and can be computed easily using simple packages such as any version of MATLAB and MATHEMATICA. These expressions can be easily used to derive very accurate and closed-form performance metrics of UWOC system which are helpful in link design techniques.

IV. COMPUTATION OF PERFORMANCE METRICS

A. TURBULENCE IN UWOC

Apart from scattering and absorption, UWOC performance gets also affected by turbulence. Turbulence in UWOC mostly arises due to rapid fluctuations in water. These rapid fluctuations leads to swift changes in the refractive index of water. It mostly occurs due to ocean currents which cause a sudden variation in temperature and pressure. Due to this sudden variation in temperature and pressure a change in refractive index occurs which leads to the oceanic turbulence. Contemplating the similarities between the atmospheric optical turbulence and underwater optical turbulence, Log-Normal turbulence model is famously used in literature [51], [52]:

$$f_h(h) = \frac{1}{h\sqrt{2\pi\sigma_x^2}} \exp\left[-\frac{(\ln h - 2\mu_x)^2}{2\sigma_x^2}\right], \qquad (32)$$

where h is the weak oceanic turbulence coefficient and μ_x and σ_x^2 are the mean and variance, respectively, of Gaussian distributed log amplitude factor $x = \ln h$. In order to make sure that the fading does not amplify and attenuate, we have

[1] The practical link length in UWOC is 20 meters [49]. We have considered 10% of this link length as small.

$$\mathrm{BSF}(\delta,\zeta_{rec}) = \frac{1}{2\pi}\sum_{i=1}^{n} w_i e^{x_i} P_{in}(\lambda)\exp\Big(\frac{-V_0(\zeta_{rec})x_i^2}{2}\Big)\exp(-c\zeta_{rec}) \times\Big\{\exp\Big[\frac{\mathcal{K}b\pi^2\zeta_{rec}}{2}{}_1F_2\Big(\frac{1}{2};\frac{3}{2},2;\frac{-x_i\zeta_{rec}^2\pi^2}{4}\Big)-\frac{0.6079b\mathcal{K}g\zeta_{rec}}{(1+g^2)}\Big]-1\Big\} \tag{30}$$

$$\mathrm{BSF}(\delta,\zeta_{rec}) = \frac{1}{2\pi}\sum_{i=1}^{n} w_i e^{x_i} P_{in}(\lambda)\exp\Big[-\frac{V_0(\zeta_{rec})x_i^2}{2}\Big]\exp(-c\zeta_{rec})\Big\{\exp\Big[\frac{\mathcal{K}b\pi^2\zeta_{rec}}{2}{}_1F_2\Big(\frac{1}{2};\frac{3}{2},2;\frac{-x_i\zeta_{rec}^2\pi^2}{4}\Big) + \sum_{m=0}^{\infty}\frac{3b\mathcal{K}g(-1)^m\pi^{2m+2}}{(1+g^2)m!\Gamma(m+1)(2m+2)} \times\Big(\frac{x_i}{2}\Big)^{2m}\frac{\zeta_{rec}^{2m+1}}{2m+1}{}_1F_2\Big(1+m;\frac{1}{2},2+m;-\frac{\pi^2}{4}\Big)\Big]-1\Big\}\sqrt{\frac{2}{\pi(x_i\delta)}}\Big(\cos\big(x_i\delta-\frac{\pi}{4}\big)\Big). \tag{31}$$

normalised the fading amplitude such that $E[h] = 1$ which results in $\mu_x = -\sigma_x^2$ [53].

B. CALCULATION OF SNR

We consider an intensity modulated/maximum likelihood (IM/ML) detection optical link with On-Off Shift keying (OOK) modulation scheme in UWOC. The optical power received at receiver in a UWOC system [23], [54] is given as follows:

$$P_{RX} = \frac{\pi\delta^2}{4}\mathrm{BSF}(\delta,\zeta_{rec}). \tag{33}$$

Here, we have assumed the channel as homogeneous downlink through the depth which means b and c are not a function of ζ_{rec}. For the simplicity of analysis, we have considered flat fading which means that the coherence bandwidth of the channel is larger than the bandwidth of the signal. The received signal at receiver is given by:

$$y = \sqrt{P_{RX}}\mathcal{R}hs + n, \tag{34}$$

where, $\mathcal{R}$ is the responsivity. The transmitted bit is represented by s; $s = 1$ when signal is present and $s = 0$ when signal is absent. The overall effect of background noise, thermal noise, and dark current in the photodetector which is modeled as additive white Gaussian noise (AWGN) is represented by n, with σ_n^2 variance. By substituting (33) in (34), the overall SNR of the system is then calculated as:

$$\gamma = \frac{\pi\delta^2\mathcal{R}^2h^2\mathrm{BSF}(\delta,\zeta_{rec})}{4\sigma_n^2}. \tag{35}$$

The pdf of SNR can be derived using transformation of random variable [55]. From (35) the cumulative distribution function (CDF) of instantaneous SNR is given by:

$$F_\gamma(\gamma) = Pr\Big[\frac{\pi\delta^2\mathcal{R}^2h^2BSF(\delta,\zeta_{rec})}{4\sigma_n^2} < \gamma\Big] = Pr\Big[h < \sqrt{\frac{4\sigma_n^2\gamma}{\pi\delta^2\mathcal{R}^2BSF(\delta,\zeta_{rec})}}\Big], \tag{36}$$

Further, we differentiate (36) to get the pdf of SNR as follows:

$$f_\gamma(\gamma) = \frac{d}{d\gamma}F_\gamma(\gamma) = \frac{1}{2\sqrt{\gamma}}\sqrt{\frac{4\sigma_n^2}{\pi\delta^2\mathcal{R}^2BSF(\delta,\zeta_{rec})}}f_h\left(\sqrt{\frac{4\gamma\sigma_n^2}{\pi\delta^2\mathcal{R}^2BSF(\delta,\zeta_{rec})}}\right). \tag{37}$$

The pdf of SNR is evaluated using (32) and (37) as follows:

$$f_\gamma(\gamma) = \frac{1}{\gamma\sqrt{8\pi\sigma_x^2}} \times\exp\left(\frac{-\left(\ln\gamma-2\mu_x+\ln\left(\frac{4\sigma_n^2}{\pi\delta^2\mathcal{R}^2BSF(\delta\zeta_{rec})}\right)\right)^2}{8\sigma_x^2}\right). \tag{38}$$

C. BER CALCULATION

The instantaneous BER of the considered system with misalignment loss [25] is given by:

$$P_e = \frac{1}{2}\,\mathrm{erfc}\,\Big(\frac{\mathcal{R}P_{RX}h}{2\sqrt{2}\sigma_n}\Big) = \frac{1}{2}\,\mathrm{erfc}\,\Big(\frac{\sqrt{\gamma}}{2\sqrt{2}}\Big), \tag{39}$$

where

$$\mathrm{erfc}(x) = \frac{2}{\sqrt{\pi}}\int_t^\infty \exp(-t^2)dt.$$

For the case when the turbulence in water is considered along with the misalignment loss in water, the BER of the considered UWOC system becomes:

$$P_e = \frac{1}{2}\int_0^\infty \mathrm{erfc}\,\Big(\frac{\sqrt{\gamma}}{2\sqrt{2}}\Big)f_\gamma(\gamma)d\gamma. \tag{40}$$

Using (23) and (40), the BER of the considered UWOC system with oceanic turbulence and misalignment loss will

be:

$$P_e = \frac{1}{2}\sum_{j=1}^{n} w_j e^{x_j}\,\mathrm{erfc}\left(\frac{\sqrt{x_j}}{2\sqrt{2}}\right)\frac{1}{x_j\sqrt{8\pi\sigma_x^2}} \times \exp\left(-\frac{\left(\ln x_j - 2\mu_x + \ln\left(\frac{4\sigma_n^2}{\pi\delta^2\mathcal{R}^2 BSF(\delta,\zeta_{rec})}\right)\right)^2}{8\sigma_x^2}\right). \quad (41)$$

D. COMPUTATION OF CAPACITY

The average channel capacity under the combined effect of turbulence and misalignment loss is defined using [56, Eq. (13)]:

$$C = \int_0^\infty \log_2(1+\gamma) f_\gamma(\gamma) d\gamma. \quad (42)$$

Using (23) and (42), the average channel capacity of the considered system is given by:

$$C = \sum_{t=1}^{n} w_t e^{x_t} \log_2(1+\gamma)\frac{1}{x_t\sqrt{8\pi\sigma_x^2}} \times \exp\left(-\frac{\left(\ln x_t - 2\mu_x + \ln\left(\frac{4\sigma_n^2}{\pi\delta^2\mathcal{R}^2 BSF(\delta,\zeta_{rec})}\right)\right)^2}{8\sigma_x^2}\right). \quad (43)$$

E. OUTAGE PROBABILITY CALCULATION

Equation (35) can be rewritten as:

$$\gamma = \frac{\pi\mathcal{R}^2\delta^2 h^2 \overline{\gamma} B\tilde{S}F(\delta,\zeta_{rec})}{4}, \quad (44)$$

where, from (25) taking $P_{in}(\lambda)$ constant, the equation of BSF can be rewritten as $\mathrm{BSF}(\delta,\zeta_{rec}) = P_{in}(\lambda)B\tilde{S}F(\delta,\zeta_{rec})$ and $\overline{\gamma} = P_{in}(\lambda)/\sigma_n^2$ is the average SNR. Since we have derived a simplified form of BSF, we can find the pdf of SNR from (44) by using transformation of random variables [55] as:

$$f_\gamma(\gamma) = \frac{1}{\gamma\sqrt{8\pi\sigma_x^2}} \exp\left(\frac{-\left(\ln\gamma - 2\mu_x + \ln\left(\frac{4}{\pi\delta^2\mathcal{R}^2\overline{\gamma}B\tilde{S}F(\delta,\zeta_{rec})}\right)\right)^2}{8\sigma_x^2}\right). \quad (45)$$

The outage probability of a system is given by [57]:

$$P_{out} = F(\gamma_{th}) = \int_0^{\gamma_{th}} f(\gamma) d\gamma. \quad (46)$$

Substituting the pdf of γ in (46) and simplifying the integration, (46) can be written as:

$$P_{out} = \int_{-\infty}^{\gamma_{th}} \frac{1}{\sqrt{2\pi}} \exp\left(\frac{-\left(\ln\gamma - 2\mu_x + \ln\left(\frac{4}{\pi\delta^2\mathcal{R}^2\overline{\gamma}B\tilde{S}F(\delta,\zeta_{rec})}\right)\right)^2}{8\sigma_x^2}\right). \quad (47)$$

Further, substituting

$$\ln\gamma - 4\mu_x + \ln(4/\pi\delta^2\overline{\gamma}B\tilde{S}F(\delta,\zeta_{rec}))/2\sigma_x = -t,$$

we can rewrite (47):

$$P_{out} = \int_{-G}^{\infty} \frac{1}{\sqrt{2\pi}} e^{-\frac{t^2}{2}} dt, \quad (48)$$

where

$$G = \frac{\ln\gamma_{th} - 2\mu_x + \ln\left(\frac{4}{\pi\delta^2\mathcal{R}^2\overline{\gamma}B\tilde{S}F(\delta,\zeta_{rec})}\right)}{2\sigma_x}. \quad (49)$$

The outage probability of the considered UWOC system with combined effects of oceanic turbulence and misalignment loss is given from (48):

$$P_{out} = Q\left(\frac{2\mu_x - \ln\left(\frac{4}{\pi\delta^2\mathcal{R}^2\overline{\gamma}_{th}B\tilde{S}F(\delta,\zeta_{rec})}\right) - \ln\gamma_{th}}{4\sigma_x}\right), \quad (50)$$

where γ_{th} is some threshold SNR and

$$Q(x) = \frac{1}{\sqrt{2\pi}}\int_x^\infty \exp\left(\frac{-u^2}{2}\right) du.$$

TABLE 2. Values of absorption, scattering and attenuation constant for different water types taken at blue/green wavelengths [24].

Water Type	$a(m^{-1})$	$b(m^{-1})$	$c(m^{-1})$
Pure sea water	0.0405	0.0025	0.043
Clean ocean	0.114	0.037	0.151
Coastal ocean	0.179	0.219	0.298
Turbid harbor	0.266	1.824	2.19

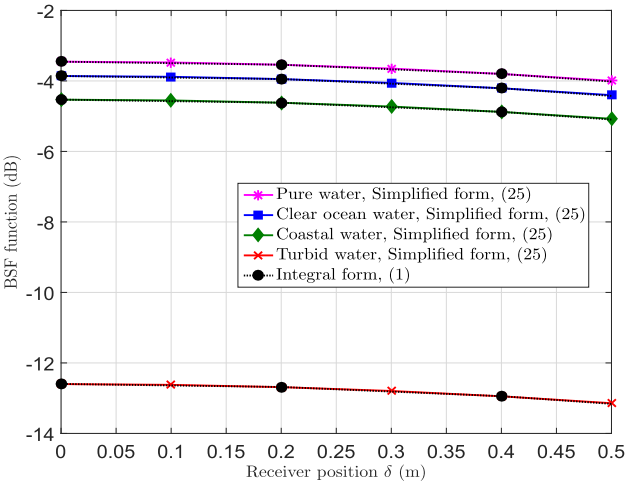

FIGURE 3. Comparison of numerically simulated (1) and analytical (25) w.r.t. receiver position δ for different values of attenuation coefficient.

V. NUMERICAL RESULTS

In this section, we will discuss the numerical results based on the expressions obtained in the previous sections. In this paper, we have considered $P_{in}(\lambda) = 3\mathrm{W}$ and $\mathcal{R} = 1$. The values of a, b, and c for different water types are shown in Table 2.

The variation of BSF with respect to (w.r.t.) different receiver position from origin is compared in Fig. 3. The

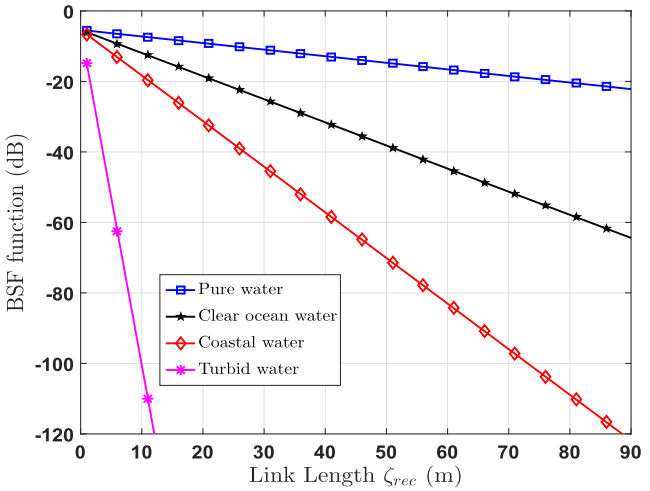

FIGURE 4. Comparison of analytical BSF w.r.t. link length ζ_{rec} for different values of attenuation coefficient.

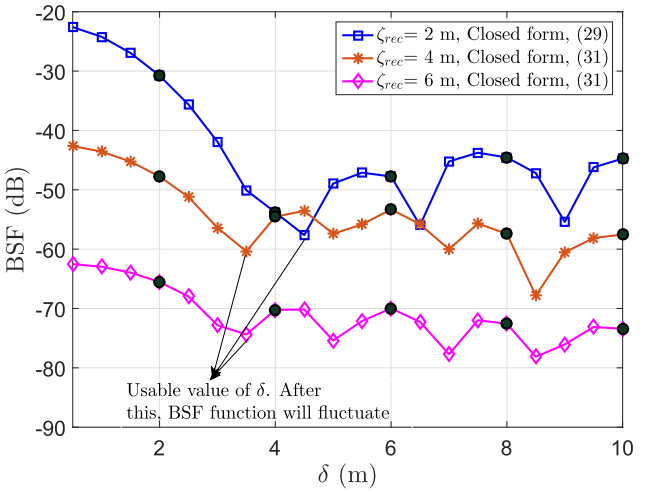

FIGURE 5. Comparison of high asymptote approximation for different values of ζ_{rec}.

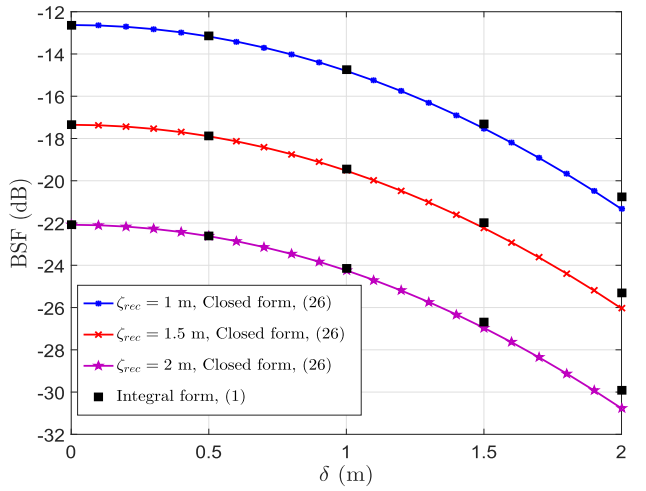

FIGURE 6. Comparison of low asymptote approximation for different values of ζ_{rec}.

integral form of BSF is plotted using (1) and the derived simplified form of BSF is plotted using (25) for different water types as mentioned in Table 2. It can be seen from the figure that the derived of BSF matches very closely to the existing integral form of BSF. It can be seen from the figure that as the quality of water degrades, the detected irradiance for a particular value of δ decreases. For example, at $\delta = 20$ cm, the detected irradiance is -3.54 dB, -3.94 dB, -4.618 dB, and -12.68 dB for pure sea water, clear ocean water, coastal water, and turbid water, respectively. In pure sea water, the effect of absorption dominates the effect of scattering, which further results in low beam divergence. Thus, as the turbidity of water increases; the amount of dissolved and suspended particles in water increases which results in more amount of photons getting scattered, rendering in the reduced received irradiance at the receiver.

Detected irradiance at the receiver which is given by BSF w.r.t. the link length ζ_{rec} plots are shown in Fig. 4 for various water types mentioned in Table 2. The BSF curves are obtained from (25). It is observed from the figure that the attenuation of incident beam increases with link length. For pure sea water, scattering coefficient is negligible because of which the beam divergence is less and thus we are able to receive light even at 90 m with a sufficient intensity. However, as the concentration of dissolved particles such as phytoplankton, detritus, and minerals increases, the value of scattering coefficient grows. Apart from being absorbed by the dissolved particles present in water, as the link length increases, more number of photons get deviated from their path and the receiver just receives the scattered part of the incident beam. This results in reduced signal levels at the receiver and can further limit the maximum data rate. Moreover, it is evident from the figure that, turbid harbor water attenuates the beam more rapidly than the other considered water types. A huge difference in the slopes of the BSF for different water types is also seen in the figure. This is because upto a certain link length the nonscattered part of light dominates the scattered part of light; but as the distance increases, the scattered part of light dominates and at a very large distance, only the scattered part of light reaches the receiver. The amount of nonscattered light reaching the receiver totally depends on the quality of water. More amount of impurities in water will lead to more scattering and less or negligible amount of nonscattered light reaches the receiver.

The verification of approximations provided in (26)–(31) is shown in Figs. 5 and 6 by plotting BSF w.r.t. δ for various values of ζ_{rec}. The water type considered is turbid harbour water. The validation of high asymptotic approximation (29) and (31) is shown in Fig. 5. It can be seen from the figure that the derived approximate form of BSF matches very closely to the integral form of BSF. As mentioned in Section III, for a high δ or ζ_{rec} or both, BSF becomes proportional to $J_0(x_i\delta)$. Hence, for a given ζ_{rec}, beyond a particular value of δ say δ_s, the BSF starts fluctuating. If δ increases further beyond δ_s for a given ζ_{rec}, the misalignment loss would be so severe that the data received at the receiver will be heavily

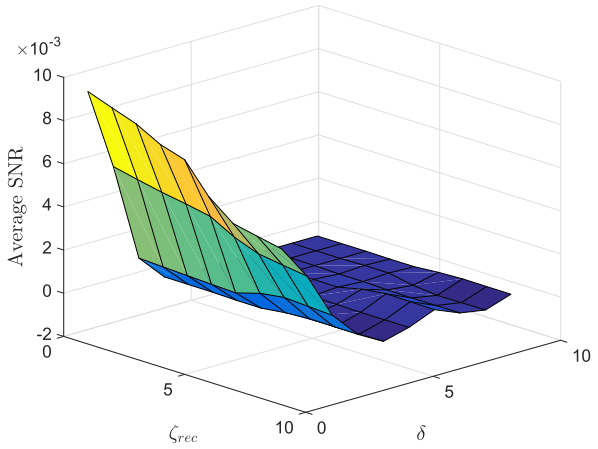

(a) SNR plot for pure water.

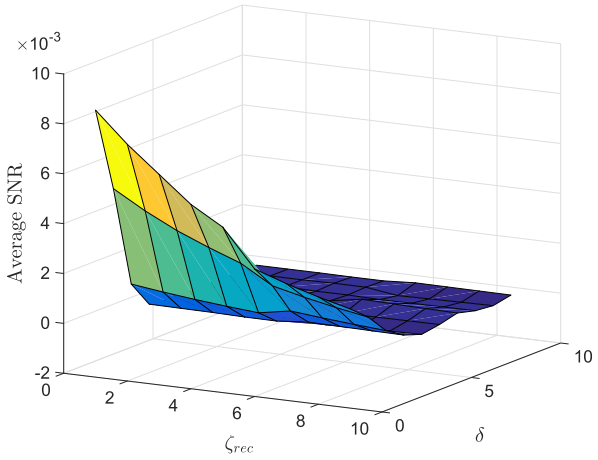

(b) SNR plot for clear ocean water.

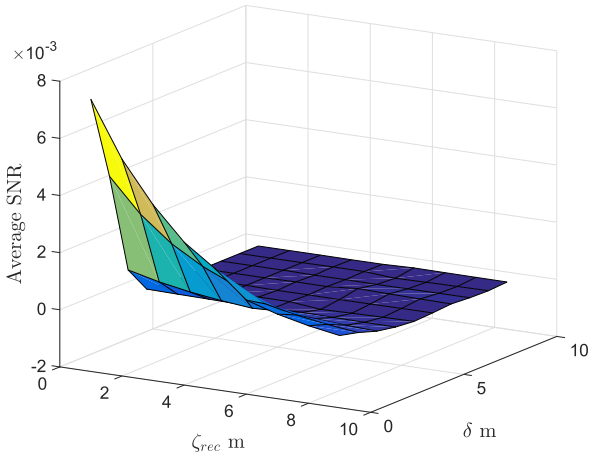

(c) SNR plot for coastal ocean water.

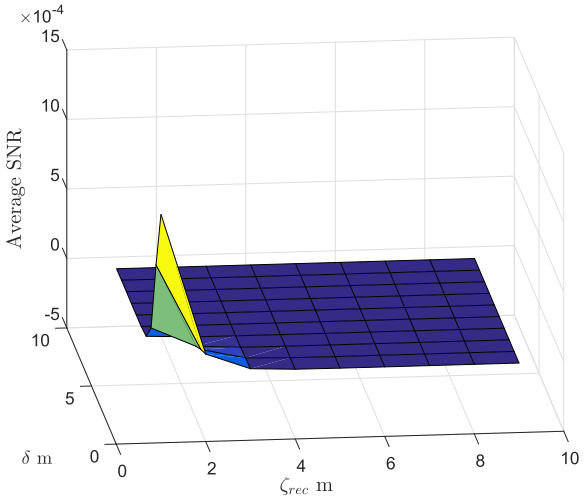

(d) SNR plot for turbid harbour water.

FIGURE 7. SNR plots for varying values of δ and ζ_{rec}.

corrupted due to fluctuations in received irradiance. This is also evident from the fluctuations in the BSF values can be seen in Fig. 5. For instance, consider the case of $\zeta_{rec} = 2$ m; in this case, ζ_{rec} is small but δ varies from 0 to 5 m. It can be seen from the figure that the BSF follows a waterfall curve till $\delta_s = 3.5$ m beyond which it starts to fluctuate. The dip observed in the figure marks the beginning of the fluctuation. If we further increase the range of δ beyond 5 m, this fluctuation will continue with continuously decreasing amplitude. For $\zeta_{rec} = 4$ m and $\zeta_{rec} = 6$ m, the high asymptote approximation curves are plotted using (31) and the value of δ_s is around 3.2 m and 3 m, respectively, as can be seen from the figure. It can also be seen from the figure that the high assymptote approximation holds good for the values of $\delta \leq 2$ m.

The low asymptotic approximation is verified in Fig. 6 by plotting the existing integral form of BSF given by (1) and the closed-form expression of BSF derived in (26). It is visible from the figure that the derived closed-form matches perfectly with the existing integral form of BSF for small values of ζ_{rec} and δ. However, as the value of ζ_{rec} and δ increases beyond 2 m, the low asymptote approximation does not hold good.

Remark 4: It should be noted that high asymptote approximate form is valid only for values of $\delta \geq 0.5$ m whereas, the low asymptote approximation is valid for $0 \leq \delta \leq 2$ m.

The effect of turbidity of water on the SNR of the considered UWOC for different water types is shown in Fig. 7. The computational curves are obtained using (44). It is noted from (44) that SNR is directly proportional to BSF; thus SNR behaves in a similar manner as BSF for high and low values of δ and ζ_{rec}. It can be seen from the figure that at high value of δ and ζ_{rec}, SNR starts fluctuating. This is because at high values of δ and ζ_{rec}, SNR becomes directly proportional to $J_0(x_i\delta)$. This insight can be easily proven from the derived approximate forms of BSF in Section III. We further observe from the figure that as the turbidity of water increases, the usable SNR area reduces. For instance, in Fig. 7(a) for pure water, SNR is maximum when $\zeta_{rec} = 1$ m and $\delta = 0$ m and it decreases uniformly till $\zeta_{rec} = 5$ m

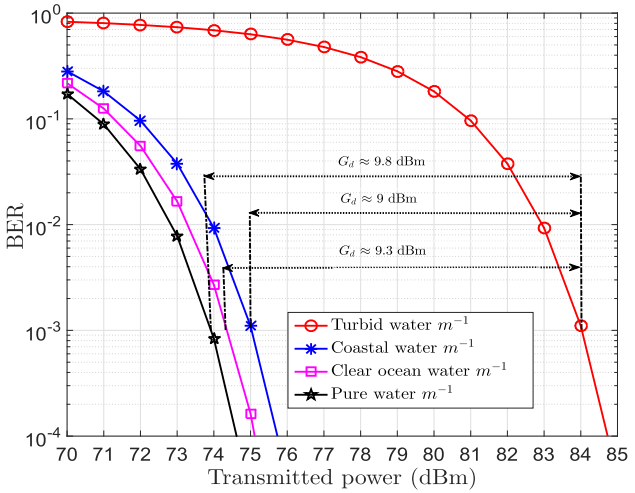

FIGURE 8. Comparison of analytical BER for different water types.

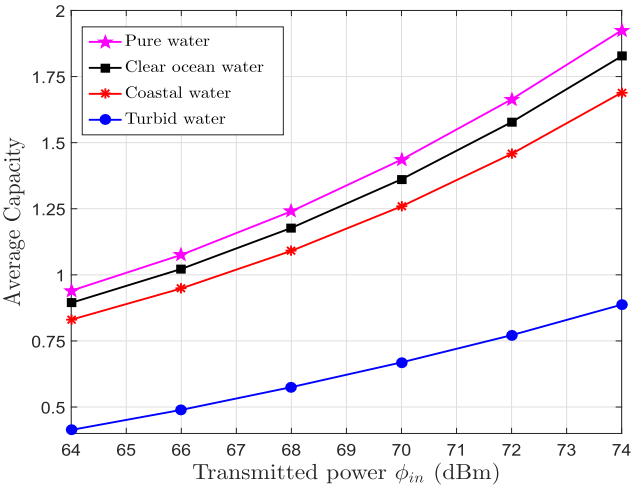

FIGURE 9. Comparison of analytical average channel capacity for different water types.

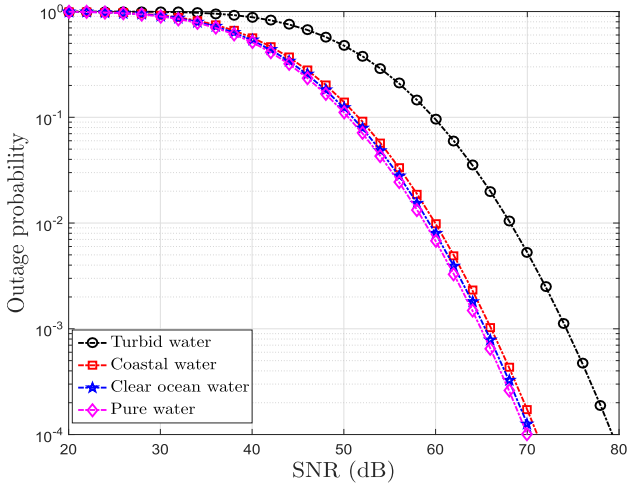

FIGURE 10. Comparison of outage probability for different water types for different water types.

and $\delta = 6$ m. However, if we increase ζ_{rec} beyond 5 m and δ beyond 6 m, SNR starts fluctuating rapidly. Similarly, for clear ocean water, decay in SNR is tolerable till $\zeta_{rec} = 5$ m and $\delta = 4$ m; for coastal ocean water, the tolerable decay in SNR is upto $\zeta_{rec} = 5$ m and $\delta = 2$ m; for turbid harbour water, tolerable decay in SNR is upto $\zeta_{rec} = 3$ m and $\delta = 1$ m. It should be noted that even though scattering helps in reducing the misalignment loss, as the water type degrades, the tolerable range of misalignment loss decreases. The exact tolerable range of ζ_{rec} and δ can be computed using the derived simplifed form of BSF given in (25).

The BER performance of the considered UWOC system with $\zeta_{rec} = 1$, $\mathcal{R} = 1$ m and $\delta = 50$ cm under the combined effect of turbulence and misalignment loss is depicted in Fig. 8. The BER curves are plotted using (41). The turbulence model is Log-Normal with $\sigma_x = 0.1$. As can be seen from the figure that the scattering and absorption coefficients greatly affect the error performance of the system. Even though the wavelength considered is in blue green region, the impurities in water affect the system BER to a huge extent. As the values of a and b increases with the intensifying concentration of dissolved and suspended particles in water, more and more photons gets deviated from their straight path. Thus, scattered light component overshadows the effect of nonscattered light component which further degrades the system performance. It can be seen from the figure that for turbid water, the BER performance is worst as compared to other water types. Turbid water suffers from power penalty[2] of 9.8 dBm, 9.3 dBm, and 9 dBm as compared to other water types. This information is useful in link designing techniques to predict the performance of the link at the initial level. For instance, turbid water will need atleast 9 dBm more power than other water types to achieve a target BER. This insight can be obtained by observing the analytical BER expression given by (41).

The effect of absorption and scattering on the average channel capacity of the considered UWOC system is shown in Fig. 9; the curves are obtained using (43). The link length of the system is 1 m with the receiver positioned at 50 cm from the origin and $\sigma_x = 0.1$. This figure shows the rate at which information can be transmitted reliably for the considered UWOC channel for a given link length and receiver offset distance. As can be seen from the figure that as the turbidity of water increases the average channel capacity of the system degrades. For instance, for a transmit power of 72 dBm, with

[2]Power penalty (G_d) means the the difference between transmitted power levels in different water types required to attain the same BER level. We have calculated SNR loss of turbid water w.r.t. other water types (as mentioned in Table 2) from Fig. 5. "For instance in Fig. 8, for $P_e = 0.0011$", in case of turbid water, the transmitted power ($P_{in,turbid}$) is $P_{in,turbid} = 84$dBm. The absolute value of transmitted power in watt is calculated as $10\log_{10}(P_{in,turbid}/10\ mW) = 10^{5.4}W$. Similarly, the absolute value of $P_{in,coastal} = 10^{4.5}W$. Now, the SNR loss in dB is given as $G_d = 10\log_{10}(P_{in,turbid}) - 10\log_{10}(P_{in,coastal}) = 9$dB. The exact transmitted power difference for different water types is clearly visible from the calculated power penalty.

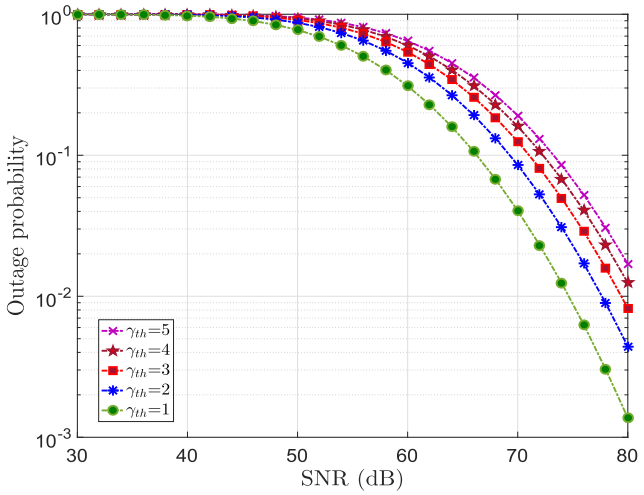

FIGURE 11. Comparison of outage probability of turbid water for different values of γ_{th}.

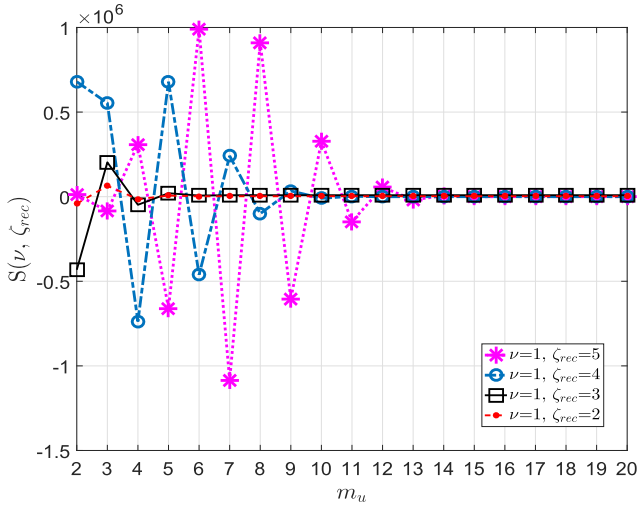

FIGURE 12. Convergence of $S(\nu, \zeta_{rec})$ for different values of ζ_{rec}.

coastal water, the average channel capacity of the system is 1.45 bits but for turbid water it drastically decays to 0.75 bits.

The outage probability as a function of average SNR for different water types is plotted in Fig. 10 for $\gamma_{th} = 2$, $\zeta_{rec} = 1$ m, and $\delta = 50$ cm. The computational curves are retrieved using (50). It is evident from the figure that the outage performance becomes better as the value of a, b and c decreases, i.e., the outage performance is the worst for the case of turbid water ($c = 2.19\ m^{-1}$) and is the best for pure sea water ($c = 0.043\ m^{-1}$). For instance, the outage probability for turbid water is 0.1 at 60 dB SNR while it is 0.1 at around 50 dB SNR for pure sea water. Thus, there is approximately 10 dB SNR improvement as the quality of water improves from turbid to pure sea water, for a given outage probability at high SNR.

The outage performance as a function of γ_{th} for turbid water for $\zeta_{rec} = 1$ m and $\delta = 0.5$ m is shown in Fig. 11. It is perceptible from the figure that as the value of γ_{th} increases, the outage performance decreases. Also, it can be seen from the figure that the system needs a minimum SNR of 40 dB to overcome the outage and become useful.

TABLE 3. Values Of m_u For different values of ζ_{rec}.

ζ_{rec}	m_u
2	3
3	5
4	7
5	13

The convergence of the infinite series in (25) which is represented as $S(\nu, \zeta_{rec})$ in (58) is shown in Fig. 12. Let the upper limit of the series be represented as m_u which shows the number of terms in the series required for convergence. For $\zeta_{rec} = 1$ m, the series converges at $m_u = 3$ and as the value of ζ_{rec} increases, the value of m_u at which the series converges also increases. Moreover, since the value $S(\nu, \zeta_{rec})$ are very small, these values are scaled by 10^6. We have given the values of m_u for different value ζ_{rec} in Table 3.

VI. CONCLUSION

A power series based simplified form of BSF, which is a measure of misalignment loss in UWOC, has been derived. Few approximations have been provided which simplify the series based expression. Using the approximations, a closed-form of BSF has been derived for a specific range of link length and receiver offset distance from the beam center. Some useful insights have been provided on the behavior of BSF for different link length and receiver offset distance condition. The proposed model has been validated through numerical results. The approximations provided have been also verified numerically. It has been confirmed via careful observations of IOPs, that the directionality of the beam is lost as the misalignment parameters increases. Using Log-Normal fading characteristics, the closed-form expressions of average BER and channel capacity have been derived and plotted for different water conditions w.r.t. the transmitted power. We have also derived the pdf of the instantaneous SNR, and using this we have obtained a closed-form expression of outage probability. Using this expression of outage probability, the results have been plotted for different water types and for different values of threshold SNR. The effect of scattering and absorption on the system performance has been studied. It has been observed through analysis that as the concentration of dissolved and suspended particles increases, the scattering of beam escalates.

APPENDIX A
DERIVATION OF (13)

The integration in (12) is given by:

$$I_2' = \int_0^{\pi} \varphi^{2m+1} \cos(\varphi) d\varphi. \tag{51}$$

Using series of $\cos(\varphi)$, the above equation can be expressed as:

$$I_2' = \sum_{n=0}^{\infty} \frac{(-1)^n \pi}{(2n)!(2m+2n+2)}. \tag{52}$$

Note that:

$$\frac{1}{(2m+2n+2)} = \frac{(m+1)_n}{(2m+2)(m+2)_n}, \tag{53}$$

where $(\cdot)_n$ represents the Pochhamer Symbol [58] and

$$(2n)! = 4^n\Big[\frac{1}{2}\big(\frac{1}{2}+1\big)\big(\frac{1}{2}+2\big)\cdots\big(\frac{1}{2}+n-1\big)\Big] \big[n(n-1)\cdots 2\cdot 1\big]. \tag{54}$$

Equation (54) can be simplified in terms of Pochhamer Symbol and is given by:

$$(2n)! = 4^n\big(\frac{1}{2}\big)_n n!. \tag{55}$$

Substituting (53) and (55) in (52) and simplifying, we obtain:

$$I_2' = \frac{\pi^{2m+2}}{(2m+2)} \sum_{n=0}^{\infty} \frac{(-1)^n}{n!}\Big(\frac{(-\pi)^2}{4}\Big)^n \frac{(m+1)_n}{\big(\frac{1}{2}\big)_n (m+2)_n}. \tag{56}$$

The series in above equation is the series of ${}_1F_2(\cdot;\cdot;\cdot)$ [33, Eq. (1)], hence (56) becomes:

$$I_2' = \frac{\pi^{2m+2}}{(2m+2)} {}_1F_2\big(1+m;\frac{1}{2},2+m;\frac{-\pi^2}{4}\big). \tag{57}$$

APPENDIX B
CONVERGENCE TEST OF INFINITE SERIES IN (25)

After writing the Hypergeometric function in the series form as given in (56), the infinite series in (25) is given by:

$$S(\nu,\zeta_{rec}) = \sum_{m=0}^{\infty} \frac{\mathcal{C}(-1)^m \pi^{2m+2}}{m!\Gamma(m+1)(2m+2)}\Big(\frac{\nu}{2}\Big)^{2m}\Big(\frac{\nu}{2}\Big)^{2m}\frac{\zeta_{rec}^{2m+1}}{2m+1} \times \sum_{n=0}^{\infty} \frac{(m+1)_n}{(\frac{1}{2})_n (m+2)_n n!}\Big(\frac{(-\pi)^2}{4}\Big)^n, \tag{58}$$

where $\mathcal{C} = 3b\mathcal{K}g(-1)^n/(1+g^2)$. The $m+1$ th and m th terms of this series are represented as a_{m+1} and a_m and are given as follows:

$$a_{m+1} = \frac{\mathcal{C}(-1)^{m+1}\pi^{2m+4}}{(m+1)!\Gamma(m+2)(2m+4)}\Big(\frac{\nu}{2}\Big)^{2m+2}\frac{\zeta_{rec}^{2m+3}}{2m+3} \times \sum_{n=0}^{\infty} \frac{(2+m)_n}{\big(\frac{1}{2}\big)_n (3+m)_n}\frac{\big(\frac{(-\pi)^2}{4}\big)^n}{n!}, \tag{59a}$$

$$a_m = \frac{\mathcal{C}(-1)^m\pi^{2m+2}}{(m)!\Gamma(m+1)(2m+2)}\Big(\frac{\nu}{2}\Big)^{2m}\frac{\zeta_{rec}^{2m+1}}{2m+1} \sum_{n=0}^{\infty} \frac{(1+m)_n}{\big(\frac{1}{2}\big)_n (2+m)_n} \times \frac{\big(\frac{(-\pi)^2}{4}\big)^n}{n!}. \tag{59b}$$

Taking ratio of (59a) and (59b) and after some manipulations, we get:

$$L = \Big|\frac{a_{m+1}}{a_m}\Big| = \Big|\frac{(-1)\pi^2\big(\frac{\nu}{2}\big)^2\zeta_{rec}^2}{(m+1)(m+1)\frac{(m+2)}{(m+1)}\frac{(2m+3)}{(2m+1)}} \times \frac{1+\frac{(1+m)}{(\frac{1}{2})(2+m)}\big(\frac{(-\pi)^2}{4}\big)+\frac{(1+m)(2+m)\big(\frac{(-\pi)^2}{4}\big)^2}{(\frac{1}{2})(\frac{3}{2})(2+m)(3+m)2!}+\cdots}{1+\frac{(2+m)}{(\frac{1}{2})(3+m)}\big(\frac{(-\pi)^2}{4}\big)+\frac{(2+m)(3+m)\big(\frac{(-\pi)^2}{4}\big)^2}{(\frac{1}{2})(\frac{3}{2})(3+m)(4+m)2!}+\cdots}\Big|. \tag{60}$$

Now applying Cauchy ratio test [59] to (60), we have

$$L' = \lim_{m\to\infty}\Big|\frac{a_{m+1}}{a_m}\Big| \to 0. \tag{61}$$

As $m \to \infty$, we see that the hypergeometric terms in numerator and denominator in (60) stay constant. Hence, as $m \to \infty$, $L \to 0$. This implies that $L < 1$. Thus, the series converges absolutely.

APPENDIX C
DERIVATION OF (18)

The integration in (17a) after substituting $\nu(\zeta_{rec}-\zeta) = t$ can be rewritten in the following way:

$$I_3' = \int_0^{\nu\zeta_{rec}} t^{-1}J_1(\pi t)dt. \tag{62}$$

Using the property of gamma function, $m! = \Gamma(m+1)$ [46] and the series form of Bessel function in (62), we obtain:

$$I_3' = \sum_{m=0}^{\infty} \frac{(-1)^m}{m!(m+1)!}\Big(\frac{\pi}{2}\Big)^{2m+1}\frac{(\nu\zeta_{rec})^{2m+1}}{2m+1}. \tag{63}$$

$1/(m+1)!$ can be alternatively written in the form of The Pochhamer symbol as:

$$\frac{1}{(m+1)!} = \frac{1}{(2)_m}. \tag{64}$$

Similarly, $1/(2m+1)$ can be represented in the form of The Pochhamer Symbol:

$$\frac{1}{2m+1} = \frac{\big(\frac{1}{2}\big)_m}{\big(\frac{3}{2}\big)_m}. \tag{65}$$

Substituting (64) and (65) in (63) we get,

$$I_3' = \frac{\pi\nu\zeta_{rec}}{2}\sum_{m=0}^{\infty}\frac{\big(\frac{1}{2}\big)_m(-1)^m\big(\frac{-\pi\nu\zeta_{rec}}{2}\big)^2 m}{m!(2)_m\big(\frac{3}{2}\big)_m}. \tag{66}$$

The series in (66) can be represented in terms of Hypergeometric function as:

$$I_3' = \frac{\pi\nu\zeta_{rec}}{2}{}_1F_2\big(\frac{1}{2};\frac{3}{2},2;\frac{-\nu^2\zeta_{rec}^2\pi^2}{4}\big). \tag{67}$$

REFERENCES

[1] C. M. G. Gussen, P. S. R. Diniz, M. L. R. Campos, W. A. Martins, and J. N. Gois, "A survey of underwater wireless communication technologies," *J. Commun. Inf. Sys.*, vol. 31, no. 1, pp. 242–255, 2016.

[2] A. Palmeiro, M. Martin, I. Crowther, and M. Rhodes, "Underwater radio frequency communications," in *Proc. OCEANS*, Jun. 2011, pp. 1–8.

[3] J. Lloret, S. Sendra, M. Ardid, and J. J. P. C. Rodrigues, "Underwater wireless sensor communications in the 2.4 GHz ISM Frequency band," *Sensors*, vol. 12, no. 4, pp. 4237–4264, Mar. 2012.

[4] I. F. Akyildiz, D. Pompili, and T. Melodia, "Underwater acoustic sensor networks: Research challenges," *Ad Hoc Netw.*, vol. 3, no. 3, pp. 257–279, Mar. 2005.

[5] J. Partan, J. Kurose, and B. N. Levine, "A survey of practical issues in underwater networks," in *Proc. ACM 1st Int. Workshop Underwater Networks (WUWNet)*, Los Angeles, CA, USA, Sep. 2006, pp. 17–24.

[6] E. M. Sozer, M. Stojanovic, and J. G. Proakis, "Underwater acoustic networks," *IEEE J. Ocean. Eng.*, vol. 25, no. 1, pp. 72–83, Jan. 2000.

[7] J. Catipovic, D. Brady, and S. Etchemendy, "Development of underwater acoustic Modems and networks," *Oceanography*, vol. 6, no. 3, pp. 112–119, Mar. 1993.

[8] M. Stojanovic, "On the relationship between capacity and distance in an underwater acoustic communication channel," *ACM SIGMOBILE Mobile Comput. Commun. Rev.*, vol. 11, no. 4, pp. 34–43, 2007.

[9] M. Stojanovic and J. Preisig, "Underwater acoustic communication channels: Propagation models and statistical characterization," *IEEE Commun. Mag.*, vol. 47, no. 1, pp. 84–89, Jan. 2009.

[10] D. Pompili and I. F. Akyildiz, "Overview of networking protocols for underwater wireless communications," *IEEE Commun. Mag.*, vol. 47, no. 1, pp. 97–102, Jan. 2009.

[11] Z. Zeng, S. Fu, H. Zhang, Y. Dong, and J. Cheng, "A survey of underwater optical wireless communications," *IEEE Commun. Surveys Tuts.*, vol. 19, no. 1, pp. 204–238, 1st Quart., 2017.

[12] B. M. Cochenour, "Experimental measurements of temporal dispersion for underwater laser communications and imaging," Ph.D. dissertation, Dept. Elect. Comp. Eng., North Carolina State Univ., Raleigh, NC, USA, 2012.

[13] L. Johnson, R. Green, and M. Leeson, "A survey of channel models for underwater optical wireless communication," in *Proc. IEEE 2nd Int. Workshop Opt. Wireless Commun. (IWOW)*, Newcastle, England, Oct. 2013, pp. 1–5.

[14] S. Jaruwatanadilok, "Underwater wireless optical communication channel modeling and performance evaluation using vector radiative transfer theory," *IEEE J. Sel. Areas Commun.*, vol. 26, no. 9, pp. 1620–1627, Dec. 2008.

[15] H. Kaushal and G. Kaddoum, "Underwater optical wireless communication," *IEEE Access*, vol. 4, pp. 1518–1547, 2016.

[16] T. C. Wu, Y. C. Chi, H. Y. Wang, C. T. Sai, and G. R. Lin, "Blue laser diode enables underwater communication at 12.4 Gbps," *Sci. Rep.*, vol. 7, 2017, Art. no. 40480.

[17] G. Baiden, Y. Bissiri, and A. Masoti, "Paving the way for a future underwater omni-directional wireless optical communication systems," *Ocean Eng.*, vol. 36, nos. 9–10, pp. 633–640, Jul. 2009.

[18] T. Hamza, M. A. Khalighi, S. Bourennane, P. Leon, and J. Opderbecke, "Investigation of solar noise impact on the performance of underwater wireless optical communication links," *Opt. Express*, vol. 24, no. 22, pp. 25832–25845, Oct. 2016.

[19] B. Cochenour, L. Mullen, A. Laux, and T. Curran, "Effects of multiple scattering on the implementation of an underwater wireless optical communications link," in *Proc. IEEE Oceans*, Boston, MA, USA, Sep. 2006, pp. 1–6.

[20] P. Saxena, A. Mathur, and M. R. Bhatnagar, "BER performance of an optically pre-amplified FSO system under turbulence and pointing errors with ASE noise," *IEEE/OSA J. Opt. Commun. Netw.*, vol. 9, no. 6, pp. 498–510, Jun. 2017.

[21] A. Jurado-Navas, J. M. Garrido-Balsells, J. F. Paris, M. Castillo-Vázquez, and A. Puerta-Notario, "Impact of pointing errors on the performance of generalized atmospheric optical channels," *Opt. Exp.*, vol. 20, no. 11, pp. 12550–12562, 2012.

[22] S. Tang, Y. Dong, and X. Zhang, "On link misalignment for underwater wireless optical communications," *IEEE Commun. Lett.*, vol. 16, no. 10, pp. 1688–1690, Oct. 2012.

[23] H. Zhang and Y. Dong, "Link misalignment for underwater wireless optical communications," in *Proc. Adv. Wireless Opt. Commun. (RTUWO)*, Nov. 2015, pp. 215–218.

[24] B. M. Cochenour, L. J. Mullen, and A. E. Laux, "Characterization of the beam-spread function for underwater wireless optical communications links," *IEEE J. Ocean. Eng.*, vol. 33, no. 4, pp. 513–521, Oct. 2008.

[25] Y. Dong, S. Tang, and X. Zhang, "Effect of random sea surface on downlink underwater wireless optical communications," *IEEE Commun. Lett.*, vol. 17, no. 11, pp. 2164–2167, Nov. 2013.

[26] N. G. Jerlov, *Marine Optimazation*, vol. 14. Amsterdam, The Netherlands: Elsevier, 1976.

[27] C. D. Mobley, *Light and Water: Radiative Transfer in Natural Waters*. New York, NY, USA: Academic, 1994.

[28] R. W. Spinard, K. L. Carder, and M. J. Perry, *Ocean Optimazation*. New York, NY, USA: Oxford Univ. Press, 1994.

[29] C. Gabriel, M. A. Khalighi, S. Bourennane, P. Leon, and V. Rigaud, "Channel modeling for underwater optical communication," in *Proc. IEEE GLOBECOM Workshops (GC Wkshps)*, Houston, TX, USA, Dec. 2011, pp. 833–837.

[30] C. Mobley, E. Boss, and C. Roesler. (2017). *Ocean Optics Web Book*. [Online]. Available: http://www.oceanopticsbook.info/ Accessed: Feb. 18, 2018.

[31] A. Morel and H. Loisel, "Apparent optical properties of oceanic water: Dependence on the molecular scattering contribution," *Appl. Opt.*, vol. 37, no. 21, pp. 4765–4776, 1998.

[32] C. Gabriel, M.-A. Khalighi, S. Bourennane, P. Leon, and V. Rigaud, "Monte-Carlo-based channel characterization for underwater optical communication systems," *J. Opt. Commun. Netw.*, vol. 5, no. 1, pp. 1–12, 2013.

[33] W. Cox and J. Muth, "Simulating channel losses in an underwater optical communication system," *J. Opt. Soc. Amer. A, Opt. Image Sci.*, vol. 31, no. 5, pp. 920–934, 2014.

[34] F. Dong, L. Xu, D. Jiang, and T. Zhang, "Monte-carlo-based impulse response modeling for underwater wireless optical communication," *Progr. Electromagn. Res.*, vol. 54, pp. 137–144, Feb. 2017.

[35] J. W. Mclean, J. D. Freeman, and R. E. Walker, "Beam spread function with time dispersion," *Appl. Opt.*, vol. 37, no. 21, pp. 4701–4711, Jul. 1998.

[36] B. Cochenour, L. Mullen, and A. Laux, "Spatial and temporal dispersion in high bandwidth underwater laser communication links," in *Proc. IEEE Military Commun. Conf.*, San Diego, CA, USA, Nov. 2008, pp. 1–7.

[37] E. P. Zege, A. P. Ivanov, and I. L. Katsev, *Image Transformation Through a Scattering Medium*, Heidelberg, Germany: Springer, 1991.

[38] J. Jaffe, "Monte Carlo modeling of underwater-image formation: Validity of the linear and small-angle approximations," *Appl. Opt.*, vol. 34, no. 24, pp. 5413–5421, Aug. 1995.

[39] J. W. Mclean, D. R. Crawford, and C. L. Hindman, "Limits of small angle scattering theory," *Appl. Opt.*, vol. 26, no. 11, pp. 2053–2054, Jun. 1987.

[40] W. H. Wells, "Theory of small angle scattering," in *Optics of the Sea* (AGARD Lecture Notes in Computer Science), vol. 61. 1973, ch. 3.3.

[41] W. H. Wells, "Loss of resolution in water as a result of multiple small-angle scattering," *J. Opt. Soc. Amer.*, vol. 59, no. 6, pp. 686–691, Jun. 1969.

[42] Y. Kuga, A. Ishimaru, H.-W. Chang, and L. Tsang, "Comparisons between the small-angle approximation and the numerical solution for radiative transfer theory," *Appl. Opt.*, vol. 25, no. 21, pp. 3803–3805, 1986.

[43] J. V. Cornacchio and R. P. Soni, "On a relation between twodimensional Fourier integrals and series of hankel transform," *J. Res. Nat. Bur. Stand. B*, vol. 69B, p. 3, Sep. 1965.

[44] D. Toublanc, "Henyey–greenstein and mie phase functions in monte carlo radiative transfer computations," *Appl. Opt.*, vol. 35, no. 18, pp. 3270–3274, Jun. 1996.

[45] D. J. Griffiths, *Introduction to Electrodynamics*. Prentice, NJ, USA: Prentice Hall, 1962.

[46] *The Wolfram Functions Site*. Accessed: Feb. 18, 2018. [Online]. Available: http://mathworld.wolfram.com/BesselFunctionoftheFirstKind. html

[47] *Nodes and Weights of Gauss-Laguerre Calculator*. Accessed: Feb. 11, 2018. [Online]. Available: http://keisan.casio.com/exec/system/1281279441

[48] *The Wolfram Functions Site*. Accessed: Feb. 11, 2018. [Online]. Available: http://mathworld.wolfram.com/Laguerre-GaussQuadrature.html

[49] C. Shen, Y. Guo, H. M. Oubei, T. K. Ng, G. Liu, K. H. Park, K. T. Ho, and M. S. Alouini, "20-meter underwater wireless optical communication link with 1.5 Gbps data rate," *Opt. Express*, vol. 24, no. 22, pp. 25502–25509, Oct. 2016.

[50] M. Abramovitz and A. Stegun, *Handbook of Mathematical Functions*. New York, NY, USA: Dover, 1965.

[51] W. Liu, Z. Xu, and L. Yang, "SIMO detection schemes for underwater optical wireless communication under turbulence," *Photon. Res.*, vol. 3, no. 3, pp. 48–53, Oct. 2015.

[52] M. V. Jamali, J. A. Salehi, and F. Akhoundi, "Performance studies of underwater wireless optical communication systems with spatial diversity: MIMO scheme," *IEEE Trans. Commun.*, vol. 65, no. 3, pp. 1176–1192, Mar. 2017.
[53] E. J. Lee and V. W. S. Chan, "Part 1: Optical communication over the clear turbulent atmospheric channel using diversity," *IEEE J. Sel. Areas Commun.*, vol. 22, no. 9, pp. 1896–1906, Nov. 2004.
[54] L. C. Andrews and R. L. Phillips, *Laser Beam Propagation Through Random Media*, 2nd ed. Bellingham, WA, USA: SPIE Press, 2005.
[55] A. Papoulis, *Probability, Random Variables, Stochastic Processes*. New York, NY, USA: McGraw-Hill, 2002.
[56] S. Anees and M. R. Bhatnagar, "On the capacity of decode-andforward dual-hop free space optical communication systems," in *Proc. IEEE Wireless Commun. Netw. Conf. (WCNC)*, Apr. 2014, pp. 18–23.
[57] S. Anees and M. R. Bhatnagar, "Performance of an amplify-andforward dual-hop asymmetric RF-FSO communication system," *IEEE J. Opt. Commu. Netw.*, vol. 7, no. 2, pp. 124–135, Feb. 2015.
[58] *The Wolfram Functions Site*. Accessed: Feb. 11, 2018. [Online]. Available: http://mathworld.wolfram.com/PochhammerSymbol.html
[59] G. Arfken, *Mathematical Methods for Physicists*, 3rd ed., Orlando, FL, USA: Academic Press, 1985.

PRAKRITI SAXENA (S'16) received the B.E. degree in electronics and communication engineering from the Medi-Caps Institute of Technology and Management, Madhya Pradesh, India, in 2014. She is currently pursuing the Ph.D. degree in optical wireless communications with the Department of Electrical Engineering, Indian Institute of Technology Delhi, New Delhi, India. Her research interests include free-space optical communication and underwater wireless optical communication.

MANAV R. BHATNAGAR (M'04–SM'13) received the M.Tech. degree in communications engineering from the Indian Institute of Technology (IIT) Delhi, New Delhi, India, in 2005, and the Ph.D. degree in wireless communications from the Department of Informatics, University of Oslo, Oslo, Norway, in 2008.

From 2008 to 2009, he was a Postdoctoral Research Fellow with the University Graduate Center (UNIK), University of Oslo. He held visiting appointments with the Wireless Research Group, IIT Delhi; the Signal Processing in Networking and Communications (SPiNCOM) Group, University of Minnesota Twin Cities, Minneapolis, MN, USA; the Alcatel-Lucent Chair, SUPELEC, France; the Department of Electrical Computer Engineering, Indian Institute of Science, Bengaluru, India; UNIK, University of Oslo; the Department of Communications and Networking, Aalto University, Espoo, Finland; and INRIA/IRISA Laboratory, University of Rennes, Lannion, France. He is currently a Professor with the Department of Electrical Engineering, IIT Delhi, New Delhi, India. He is also a Brigadier Bhopinder Singh Chair Professor there. His research interests include signal processing for multiple-input-multiple-output systems, cooperative communications, noncoherent communication systems, distributed signal processing for cooperative networks, multiuser communications, ultrawideband-based communications, free-space optical communication, cognitive radio, software-defined radio, power line communications, smart grid communications, physical layer security, molecular communications, and satellite communications.

Dr. Bhatnagar is a Fellow of the Institution of Engineering and Technology, U.K., the Indian National Academy of Engineering, the National Academy of Sciences, India, the Institution of Electronics and Telecommunication Engineers, India, and the Optical Society of India. He was a recipient of the NASI-Scopus Young Scientist Award 2016 in the engineering category and the Shri Om Prakash Bhasin Award in the field of Electronics and Information Technology in 2016. He was selected as an Exemplary Reviewer of the IEEE COMMUNICATIONS LETTERS from 2010 to 2012, and the IEEE TRANSACTIONS ON COMMUNICATIONS, in 2015. He was an Editor of the IEEE TRANSACTIONS ON WIRELESS COMMUNICATIONS, from 2011 to 2014.